CANCER

Multiplex digital profiling of DNA methylation heterogeneity for sensitive and cost-effective cancer detection in low-volume liquid biopsies

Yang Zhao[1], Christine M. O'Keefe[1], Jiumei Hu[2], Conor M. Allan[2], Weiwen Cui[1], Hanran Lei[1], Allyson Chiu[1], Kuangwen Hsieh[2], Sonali C. Joyce[3], James G. Herman[3], Thomas R. Pisanic[4,5]*, Tza-Huei Wang[1,2,4,5]*

Molecular alterations in cancerous tissues exhibit intercellular genetic and epigenetic heterogeneity, complicating the performance of diagnostic assays, particularly for early cancer detection. Conventional liquid biopsy methods have limited sensitivity and/or ability to assess epigenetic heterogeneity of rare epiallelic variants cost-effectively. We report an approach, named REM-DREAMing (Ratiometric-Encoded Multiplex Discrimination of Rare EpiAlleles by Melt), which leverages a digital microfluidic platform that incorporates a ratiometric fluorescence multiplex detection scheme and precise digital high-resolution melt analysis to enable low-cost, parallelized analysis of heterogeneous methylation patterns on a molecule-by-molecule basis for the detection of cancer in liquid biopsies. We applied the platform to simultaneously assess intermolecular epigenetic heterogeneity in five methylation biomarkers for improved, blood-based screening for early-stage non–small cell lung cancer. In a cohort of 48 low-volume liquid biopsy specimens from patients with indeterminant pulmonary nodules, we show that assessment of intermolecular methylation density distributions can notably improve the performance of multigene methylation biomarker panels for the early detection of cancer.

INTRODUCTION

DNA methylation is a primary means of controlling cellular gene expression and the most widely studied form of epigenetic modification to date (*1*). Numerous studies have demonstrated that virtually all human cancers exhibit aberrant DNA methylation, which can often contribute to carcinogenesis and subsequent therapeutic resistance (*2*, *3*). The accrual of aberrant DNA methylation, particularly within CpG (*5′-C-phosphate-G-3′*) islands of gene promoter regions, often occurs at early stages of, and even before carcinogenesis, making DNA methylation a highly attractive biomarker for detecting early-stage cancers (*4*). However, assessment of DNA methylation at early stages can be complicated by the fact that the methylation patterns themselves evolve progressively and stochastically throughout the genome, resulting in a high degree of intercellular methylation heterogeneity (*5*–*8*). The occurrence of these processes in both cancerous, and to a lesser extent, healthy tissues [e.g., cell cycle or age-related epigenetic drift (*9*)], can reduce the clinical sensitivity and specificity of diagnostic assays and undermine the utility of DNA methylation biomarkers for early-stage cancer detection and screening applications, in particular. Likewise, new methods are needed that can comprehensively sample methylation heterogeneity and epiallelic distributions at sufficient resolution and low cost to better leverage methylation biomarkers for improved detection of early-stage or low-volume tumors (*10*).

Numerous studies have demonstrated that liquid biopsies of peripheral blood (as well as other body fluids such as urine or stool) contain cell-free DNA (cfDNA) derived from tissues throughout the entire body. In patients with cancer, liquid biopsies also contain circulating tumor DNA (ctDNA) with molecular alterations that reflect those found in the cancerous tissue sources themselves (*11*–*14*). Though promising, ctDNA exhibiting such molecular alterations can be exceedingly rare, and is often only present in variant allele (or epiallele) frequencies of 0.1% or lower (*15*, *16*). Therefore, detection of these rare and sporadic heterogeneously methylated epialleles specific to tumors requires the development of methods that provide high sensitivity, specificity, and resolution, while being sufficiently simple and affordable to allow for integration into routine diagnostic and screening practices.

DNA methylation analysis has been substantially advanced by methods such as polymerase chain reaction (PCR)–based approaches and next-generation sequencing (NGS) technologies. PCR-based techniques, including droplet digital methylation-specific PCR (ddMSP) and MethyLight, can detect hyper- or hypomethylation of loci in fractions as low as 0.01% but cannot reliably detect or quantify heterogeneous methylation patterns (*17*–*23*). Furthermore, fundamental technical constraints have limited most digital PCR (dPCR) methods to the analysis of four or fewer loci per assay (*24*, *25*). Alternatively, NGS-based approaches including bisulfite sequencing (*26*, *27*) and microarray-based analyses, such as the Infinium MethylationEPIC BeadArray (Illumina) (*28*, *29*), provide comprehensive analysis of DNA methylation and epigenetic patterns, respectively, across the genomic landscape, yet require high levels of input DNA (e.g., 20 ml of plasma) and face challenges in detecting epiallelic fractions lower than 0.1% (*30*–*32*). While several well-documented sequencing-based approaches have recently been developed to improve clinical sensitivity through the use of large biomarker panels (*33*, *34*), these techniques are currently not cost-effective for routine screening applications and require substantial amount of input DNA, substantial expertise, sample preparation, and time to implement.

[1]Department of Biomedical Engineering, Johns Hopkins University, Baltimore, MD 21218, USA. [2]Department of Mechanical Engineering, Johns Hopkins University, Baltimore, MD 21218, USA. [3]Division of Hematology and Oncology, Department of Medicine, University of Pittsburgh Medical Center, Pittsburgh, PA 15261, USA. [4]Johns Hopkins Institute for NanoBioTechnology, Johns Hopkins University, Baltimore, MD 21218, USA. [5]Department of Oncology, The Sidney Kimmel Comprehensive Cancer Center at Johns Hopkins, Baltimore, MD 21287, USA.
*Corresponding author. Email: thwang@jhu.edu (T.-H.W.); tpisanic@jhu.edu (T.R.P.)

Methylation-sensitive high-resolution melting analysis (MS-HRM) is a bulk post-PCR technique that is used to assess the methylation status of amplicons derived from bisulfite-treated (BST) template DNA by monitoring their denaturation as a function of temperature (*35*–*37*). In prior work, we expanded on this approach by developing an improved method called DREAMing (Discrimination of Rare EpiAlleles by Melt) that allows locus-specific detection and analysis of heterogeneous methylation patterns of rare copies of ctDNA epiallelic variants (*38*). We subsequently demonstrated that the DREAMing assay could be implemented with a 4096-nanowell digital microfluidic device to expand the dynamic range, allowing quantification of epialleles over four orders of magnitude even in the presence of a background of 2 million unmethylated targets (0.00005%) (*39*). Nonetheless, a seemingly fundamental limitation common to DREAMing and other HRM-based techniques is their general inability to be parallelized for multiplexed analysis of biomarker panels, greatly reducing throughput, and limiting translational potential. Molecular probes like TaqMan probes, which are commonly used to identify only fully methylated biomarker loci in multiplex methylation-specific PCR (MSP) or digital MSP assays, are generally incompatible with HRM-based methods due to the need to detect heterogeneous methylation patterns. As a result, despite the high sensitivity to detect or quantify heterogeneous methylation patterns, HRM-based and digital HRM-based methods have historically been limited to single-plex detection.

Here, we present an approach called REM-DREAMing (Ratiometric-Encoded Multiplex Discrimination of Rare EpiAlleles by Melt) that provides a simple and cost-effective means of achieving highly sensitive, multiplex analysis of intermolecular epiallelic heterogeneity at single-copy resolution. REM-DREAMing uses a ratiometric fluorescence labeling technique with methylation-agnostic probes and precise digital high-resolution melt (dHRM) analysis to allow concurrent differentiation and analysis of methylation patterns on a copy-by-copy basis for all loci in the panel. The REM-DREAMing platform employs digital microfluidics comprising four independent but identical modules, each containing 10,400 nanowells to provide sufficient digitization power enabling performance of multiple highly multiplexed assays in parallel. To demonstrate the utility of REM-DREAMing, here we design and evaluate a multiplex dHRM assay for assessing and leveraging intermolecular methylation heterogeneity in a panel of five biomarkers previously investigated for early detection of non–small cell lung cancer (NSCLC). Using a group of 48 low-volume liquid biopsy samples sourced from individuals with computed tomography (CT) scan indeterminate pulmonary nodules, our study reveals that a notable improvement in performance over traditional methylation assessment techniques can be achieved through the assessment of intermolecular methylation density distributions across multigene panels, achieving a clinical sensitivity of 93% at 90% clinical specificity and an overall area under the receiver operating characteristic (ROC) curve (AUC) of 0.96 [95% confidence interval (CI), 0.91 to 1].

RESULTS

Overview of the REM-DREAMing platform

REM-DREAMing uses a ratiometric fluorescence labeling scheme with dHRM analysis to achieve simultaneous assessment of epigenetic heterogeneity on a copy-by-copy basis for a given panel of methylation biomarkers. A general overview of the REM-DREAMing platform is shown in Fig. 1. Circulating cfDNA is first extracted from peripheral blood liquid biopsy specimens by magnetic silica beads and undergoes bisulfite conversion (Fig. 1A) (*39*–*42*). Bisulfite treatment is used to convert unmethylated cytosine residues to uracil

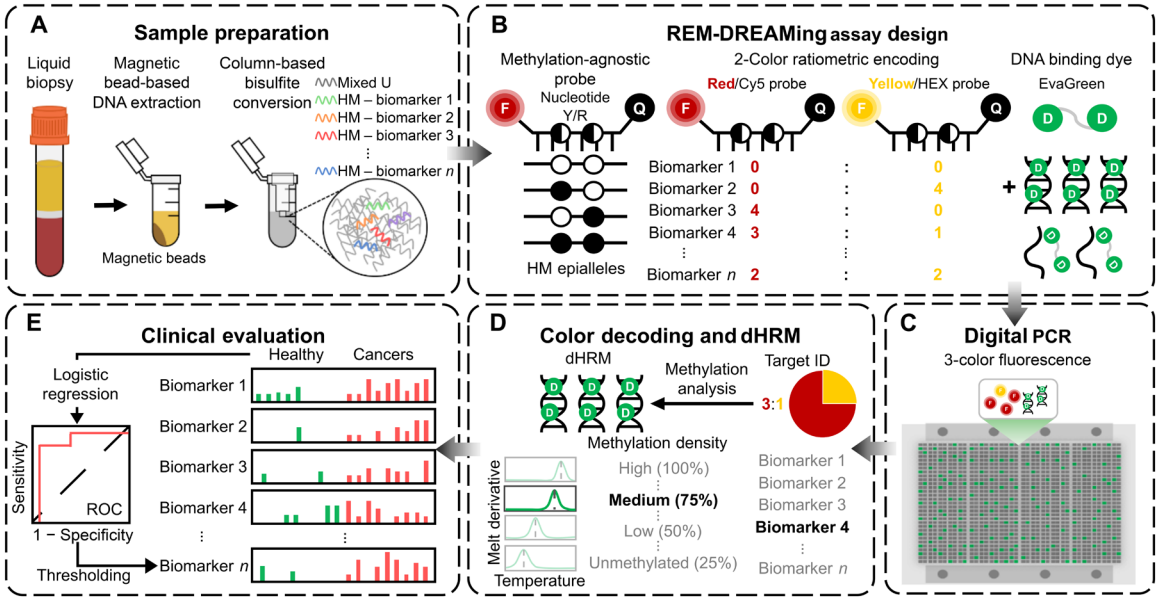

Fig. 1. REM-DREAMing overview. (**A**) DNA is extracted from a liquid biopsy specimen and undergoes bisulfite conversion treatment. (**B**) The sample containing a heterogeneous population of converted epialleles is added to a PCR mix containing pairs of methylation-agnostic probes labeled with red or yellow fluorophores and quenchers and DNA binding dye, specifically EvaGreen. (**C** and **D**) Following absolute digitization in a microfluidic chip and dPCR, each amplified target is identified by its distinct red-to-yellow fluorescence signature ratio. The subsequent EvaGreen-based dHRM analysis measures the melting temperature of the DNA target, thereby determining the methylation density of amplified target. (**E**) Detected epialleles with methylation densities greater than the predetermined threshold are tallied and fed into a logistic regression model to predict the cancer status of the sample.

while methylated (CpG-dinucleotide) cytosine residues remain unchanged, thus directly translating DNA methylation patterns into corresponding changes in the primary sequences of the template molecules. REM-DREAMing assesses heterogeneous methylation patterns by leveraging thermodynamic differences of amplicons derived from bisulfite-converted template molecules to quantify the fraction of methylated CpGs (or methylation density) from each individual/digitized template copy. Specifically, bisulfite-induced changes from cytosine to uracil alter nucleic acid base stacking (*43*) and decrease the thermodynamic stability of the double-stranded DNA (dsDNA), resulting in a measurable shift in the temperature at which a sequence denatures, termed the amplicon melt temperature T_m (fig. S1). Compared to unmethylated epialleles, the observed melt temperature of amplified methylated epialleles increases proportionally to the number of methylated CpG dinucleotides (viz. methylation density) in the respective template molecules (figs. S3 and S4). Thus, the combination of single-copy sensitive digital assays with parallelized assessment of melt temperature on a molecule-by-molecule basis allows rapid comprehensive epiallelic profiling of all target molecules in the sample.

To enable the simultaneous assessment of multiple methylation biomarkers, REM-DREAMing introduces a probe-based ratiometric fluorescence labeling approach to the dHRM assay. A key challenge in using probe-based methods for detecting heterogeneous DNA methylation is the requirement for defined target sequence. However, bisulfite conversion of a given epiallelic target template molecule yields any one of 2^n possible sequence permutations, where n is the number of CpG sites in the target locus. To resolve this issue, methylation-agnostic probes were designed by incorporating degenerate bases [Y (C or T) or R (G or A)] complementary to each methylation-dependent (CpG) base in the target sequence, thereby enabling hybridization to the target locus, regardless of the epiallelic methylation pattern. Moreover, the spectral overlap of fluorophores has traditionally limited the ability to achieve prominent levels of multiplexing in fluorescence probe-based assays. REM-DREAMing overcomes this through a ratiometric fluorophore labeling technique to achieve expanded levels of multiplexing capability. Briefly, identical TaqMan probes are designed against each respective target sequence but are synthesized with either red/Cy5 or yellow/HEX fluorophores and quenchers, which allow the probes to be mixed at a predefined stoichiometric ratio to create a locus-specific dual-color ratiometric fluorescence signature (Fig. 1B). Multiplexing is then achieved by adding probe pairs, each with a unique red-to-yellow molar ratio, for each respective target in the panel of interest, which can then be identified post-PCR by two-channel fluorescence analysis. The coupling of the ratiometric fluorescence encoding technique with methylation-agnostic probe design thus permits multiplexing while maintaining compatibility with DNA binding dyes, such as EvaGreen, thereby enabling simultaneous identification and methylation heterogeneity analysis of epiallelic gene target panels.

Digitization of extracted, bisulfite-converted DNA on the REM-DREAMing platform is accomplished by loading samples onto a microfluidic device comprising four modules, each holding 10,400 2.5-nl nanowells that are used to effectively digitize all template molecules into discrete reaction chambers. Following dPCR on the microfluidic device, each PCR-amplified target can be identified by its distinct fluorescence signature ratio (Fig. 1, C and D). Subsequent EvaGreen-based dHRM analysis is then used to determine the T_m of the amplified DNA target, from which the methylation density of original template molecule in each nanowell can be directly inferred (Fig. 1D). A "DREAM analysis" frequency histogram describes the observed frequency of each methylation-density variant, which can then be plotted to visualize a given sample's epigenetic heterogeneity at each target locus in the biomarker panel. Last, a multivariate logistic regression (or other) model can be constructed based on statistical differences in single-molecule sample methylation density distributions to identify ideal thresholds of the biomarker panel for distinguishing healthy controls and cancer cases (Fig. 1E).

Microfluidic device design and operation

The REM-DREAMing microfluidic device was designed to provide substantial improvements over our previously reported microfluidic device (*39*), which used an ultrathin soft lithography method that alleviates evaporation loss during thermocycling and reduces optical scattering over traditional designs (Fig. 2A). Nonetheless, this design exhibited several limitations, most notably a sample loading efficiency of 10% and a single module housing 4096 wells limited its utility for multiplex assays due to its low digitization power. In contrast, the REM-DREAMing platform includes several key amendments to enable the performance of parallelized DREAMing of panels containing multiple methylation biomarkers. Overall, the REM-DREAMing microfluidic array was designed to meet three key parameters: (i) sample loss less than 10% during oil partitioning; (ii) ability to accommodate three or more replicates/samples; and (iii) sufficient digitization power to simultaneously assess and quantify a panel of four or more biomarkers.

The poor loading efficiency of the previous chip design was primarily due to losses in the loading channels. We thus optimized the height difference between the nanowells and channels to substantially improve the loading efficiency while also ensuring the structural robustness of the device. By introducing a height difference between the nanowells and channels (aspect ratio), the volume ratio between nanowells and channels could be increased from 1:1 to 9:1, resulting in a loading efficiency of approximately 90%, or a ninefold improvement over the previous design (Fig. 2A). Another issue that has plagued many digital platforms is sample throughput. To address this issue, some commercial devices, such as Crystal dPCR chip from Stilla (*44*, *45*) and QIAcuity from Qiagen, have been developed with multiple microfluidic modules or compartments to achieve parallelized sample analysis (*46*, *47*). Similarly, we designed incorporation of four independent but identical modules into the REM-DREAMing microfluidic device to enable simultaneous analysis of sample replicates or up to four independent samples (Fig. 2B).

Beyond parallelization, an important aspect of digital analysis techniques is ensuring that the number of microchambers and input number of targets are matched to ensure accurate quantification. Specifically, Poisson statistics can be used to determine the probability, P, of a nanowell containing k number of target molecules, as follows (*48*, *49*)

$$P(k) = \frac{e^{-\lambda}\lambda^k}{k!}, k = 0, 1, 2, 3 \quad (1)$$

where λ is the number of copies of target molecule per nanowell.

Similarly, multiplex digital assays require that all target species are sufficiently digitized to enable accurate quantification of all target molecules. To meet this requirement, we calculated the λ value in an n-plex assay based on setting the probability that each nanowell only

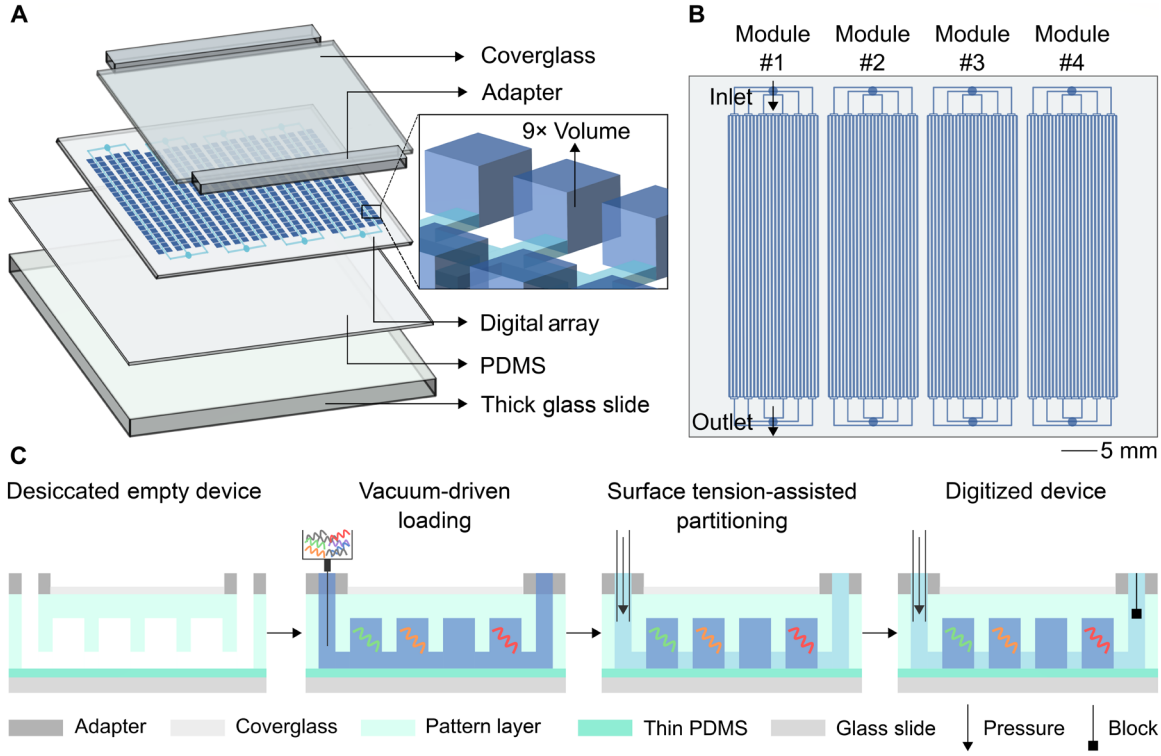

Fig. 2. Microfluidic device design and operation. (**A**) The microfluidic device is composed of four layers: a PDMS-coated thick glass slide, an ultra-thin PDMS layer, a PDMS pattern layer, and a thin glass coverslip between adapters accommodating inlets and outlets. The height of nanowells and channels (aspect ratio) is 150 and 50 μm, respectively, resulting in a ninefold increase in sample loading efficiency compared to the previous designs. (**B**) Each device comprises four independent modules, and each module holds 10,400 2.5-nl nanowells. (**C**) Samples are rapidly drawn into the device, which has been desiccated to create a negative pressure differential. A partitioning liquid is then injected into the inlet to achieve absolute digitization of DNA fragments. The device is maintained under pressure to lock the digitized sample in place during PCR.

has zero or one target ($k = 0$ or 1) to be 95% (only 5% of nanowells will have more than one molecule) as follows

$$P = n\left[P(k=0)+P(k=1)\right] = n(e^{-\lambda}+\lambda e^{-\lambda}) = n\left[(1+\lambda)e^{-\lambda}\right] \quad (2)$$

For a five-plex assay, λ values ≤0.071 are sufficient to achieve absolute digitization of ≥95% of all template molecules. To fulfill the requirements of assaying up to 1000 target copies, we designed our microfluidic device to have 10,400 nanowells in each respective module. Multiple modules or devices can be used in parallel to increase clinical sensitivity and/or accommodate higher cfDNA concentrations.

Sample digitization and chip imaging (Fig. 2C) were performed using our previously published protocol (*42*). The device incorporates a rapid, vacuum-assisted loading mechanism, allowing sample loading and digitization to be performed in under 15 s. Digitization relies on surface tension and pressure-driven partitioning of an oil-based solution through the microchannels to isolate the reaction chambers. To prevent sample leakage during PCR, partitioning oil is kept under pressure. The partitioning oil also contains polydimethylsiloxane (PDMS), which solidifies during PCR to produce a physical barrier between reaction chambers. This technique ensures that the microfluidic device can be easily handled for digital melting and fluorescence imaging analyses without requiring continuous pressurization, while also minimizing the risk of contamination. Endpoint fluorescence imaging was achieved using a flatbed fluorescence scanner, which uses lasers paired with emission filters matched to the excitation and emission spectra of the DNA binding dye (EvaGreen) and each respective fluorophore. To perform dHRM, we developed a thermal optical platform consisting of a flatbed thermal cycler and a wide-field imager that captures fluorescence images of the entire array at temperature increments of 0.1°C.

Ratiometric fluorescence labeling validation

We first sought to assess the ability of ratiometric fluorescence encoding to effectively differentiate amplified target species. Technical validation of the technique was performed by introducing synthetic DNA sequences, equivalent to bisulfite-converted fully methylated and unmethylated epialleles of *CDO1*, into a single module on the microfluidic device along with the corresponding the *CDO1* DREAMing primer pair and Cy5- or HEX- labeled TaqMan probes at predefined concentration ratios (4:0, 3:1, 2:0, 0:0, 0:2, 0:4, 1:3, and 2:2). Following dPCR on chip, amplification was identified by positive EvaGreen fluorescence signal in a given nanowell. The endpoint fluorescence signal of all positive nanowells is shown in fig. S6 along with the color-coded Cy5 (red) and HEX (yellow) fluorescence images. Our results indicate that at least eight ratiometric codes could be reliably distinguished providing the ability to perform parallelized digital analysis on up to eight targets with only two fluorophore colors (Fig. 3A). While we limited our validation to two colors for proof of concept, our preliminary data strongly suggest that higher

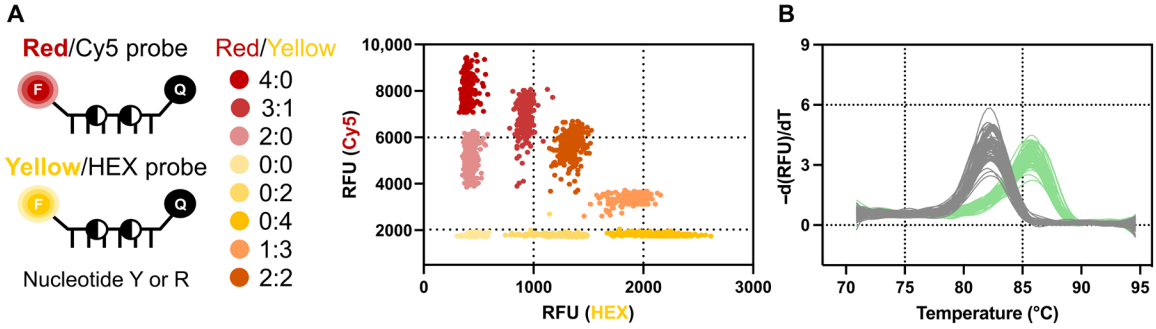

Fig. 3. Ratiometric labeling validation for REM-DREAMing. (**A**) Eight different ratios (4:0, 3:1, 2:0, 0:0, 0:2, 0:4, 1:3, and 0:0) can be distinguished by two TaqMan probes labeled with either Cy5 or HEX fluorophores and quenchers. (**B**) Representative melt curve derivatives from experiments with a 4:0 Cy5 to HEX ratio for synthetic DNA molecules equivalent to converted fully methylated (labeled in green color) and unmethylated (labeled in gray color) epialleles.

degrees of multiplexing can be readily achieved by using more fluorophores/channels. Extrapolation from our initial results indicates that 35 targets could be reliably distinguished by adding only one additional spectrally distinct fluorophore (such as Texas Red). Nonetheless, our results indicate that the variance of fluorescence intensities can be target-assay dependent and thus additional ratiometric codes may lead to overlapping clusters on the fluorescence map. These issues can often be resolved by simply fine-tuning the assay conditions, including probe concentration and PCR conditions, to reduce variance and enhance confidence levels.

We next sought to validate that the ratiometric detection scheme could be used without interfering with EvaGreen-based DREAMing analysis of methylation density. This was achieved by adding synthetic DNA sequences equivalent to bisulfite-converted fully methylated and unmethylated epialleles to the reaction mixture. The representative traces of fluorescence signals from individual wells are shown in Fig. 3B and were classified by melting temperatures via thresholding and color coded by methylation density. The presence of two clearly distinct melt curves indicated methylation-independent amplification of both fully methylated and unmethylated template molecules.

REM-DREAMing clinical validation

Having demonstrated the multiplexing and methylation assessment capacity of REM-DREAMing for at least eight targets using only two fluorophore colors, we next aimed to preliminarily assess the performance of the assay platform in a clinically relevant application. Toward this end, we developed a five-plex REM-DREAMing liquid biopsy assay targeting a five-gene panel of DNA methylation biomarkers that had previously shown promise for NSCLC screening applications. This panel was originally selected based on examination of data from The Cancer Genome Atlas. In particular, the genome-wide methylomic data from Illumina 450K Methylation analysis of NSCLC and matched normal lung was used to identify loci exhibiting prevalent, NSCLC-specific hypermethylation within CpG islands of gene promoter regions (*50*). The biomarker panel comprising five genes (*CDO1*, *TAC1*, *HOXA7*, *HOXA9*, and *SOX17*) was clinically validated by implementing single-plex, real-time methylation-specific PCR (MethyLight) (*19*, *51*) assays in a case-control study of liquid biopsies from a cohort of high-risk patients in which indeterminant pulmonary lung nodules were identified by low-dose CT scan screening (*17*). The results of this study confirmed that hypermethylation in these loci could be detected much more frequently in cfDNA derived from patients with NSCLC when compared to samples derived from patients with no or benign disease (*17*, *18*). While these results were promising, we reasoned that the inability of traditional MSP approaches like MethyLight to detect partial, or heterogeneous, methylation might compromise the clinical performance of the panel (*52*). To test this hypothesis, we created a single, multiplex REM-DREAMing assay targeting the five-gene panel to explore whether the uniquely rich data afforded by the digital assessment of heterogeneous methylation could be leveraged to further improve clinical performance.

For the creation of the NSCLC REM-DREAMing assay, we first designed a five-plex DREAMing assay according to the design guidelines described above. We then validated the analytical performance of the assay using synthetic DNA sequences equivalent to bisulfite-converted fully methylated and unmethylated epialleles of each target in the gene panel. The synthetic templates were added into a single reaction mixture along with all five primer pairs and Cy5- or HEX-labeled TaqMan probes at a predefined concentration ratio (0:9, 0:5, 5:0, 9:0, or 0:0) for each respective target locus (table S1). Following dPCR on chip, positive amplification could be readily identified by strong EvaGreen fluorescence signals within the nanowells (Fig. 4A, top). The endpoint fluorescence signals from individual nanowells are shown in Fig. 4 (A and B), which are color coded into five populations based on their dual color (red/Cy5 and yellow/HEX fluorophores) ratiometric fluorescence signatures. Positive wells were determined by the presence of EvaGreen signals and peaks in the negative derivative of their respective melt curves. To distinguish the five ratiometric-labeled populations, a Gaussian Mixture Model (GMM) was applied to the fluorescence intensity values for each fluorescence channel to assign each data point to an appropriate cluster. The resulting data demonstrate that the GMM results in five differentiable signal clusters (fig. S2). The fluorescence signature corresponding to each respective biomarker could be readily distinguished based on the respective Cy5-to-HEX ratios observed in the positive sample wells (Fig. 4B). Within each cluster, the negative derivative melt peaks derived from the EvaGreen-based dHRM analysis determined the methylation density of each amplicon (Fig. 4C). As expected, each positive nanowell exhibited a melt temperature corresponding to either a fully methylated or fully unmethylated variant.

We next validated the analytical performance of our five-plex REM-DREAMing platform by constructing a standard curve using synthetic DNA sequences equivalent to bisulfite-converted, fully methylated epialleles in concentrations ranging from 0 to 150 copies per reaction module. Fixed numbers of synthetic copies equivalent to

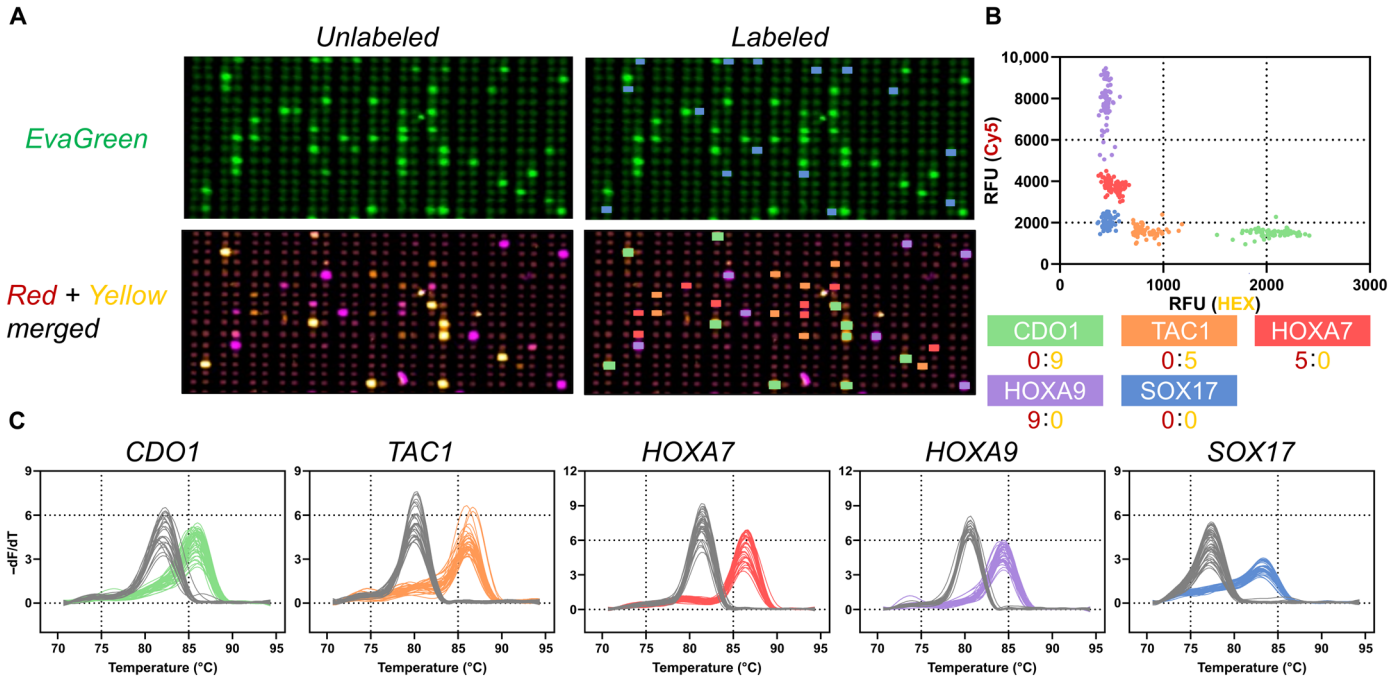

Fig. 4. Five-plex REM-DREAMing validation. (**A**) Representative micrographs of subsets of the EvaGreen and merged red and yellow color-coded fluorescence images of the chip showing multiplexed detection of *CDO1* (green), *TAC1* (orange), *HOXA7* (red), *HOXA9* (purple), and *SOX17* (blue) on chip. (**B**) Five clusters are identified by applying a GMM to the two-dimensional signal intensity dot plots. The red/Cy5 and yellow/HEX fluorophore ratio of each cluster is shown below. (**C**) Representative melt curve derivatives of fully methylated (color coded) and fully unmethylated (labeled in gray color) epialleles.

converted unmethylated epialleles were also added to the reaction mixture. Linear fits from 0 to 150 copies produced slopes in the range of 0.80 and 0.85 (Fig. 5). This discrepancy is consistent with our previous "HYPER-Melt" design and is likely attributable to well shrinkage due to inelastic deformation of PDMS under vacuum (*53*). Linear fits of the standard curves exhibited R^2 values ≥0.98, suggesting that REM-DREAMing provides strong absolute quantitation capability across a broad range of target concentrations. Results of this validation demonstrate that by coupling a ratiometric fluorescence labeling technique and dHRM analysis, REM-DREAMing platform provides simultaneous methylation detection of five biomarkers at single-copy sensitivity.

Multiplexed detection of methylation biomarkers in plasma

We next sought to preliminarily assess the diagnostic potential of the five-plex NSCLC REM-DREAMing assay by comparing the epiallelic distributions of the five target loci in 48 DNA samples derived from liquid biopsy specimens collected from patients with CT scan–identified indeterminate pulmonary nodules. Overall, the cohort comprised 24 patients who were later diagnosed with early-stage (I or II) NSCLC, 5 diagnosed with late-stage (III or IV) NSCLC and 19 with nodules subsequently confirmed as benign upon pathological examination (table S2). Representative REM-DREAMing analyses of the five-gene panel from cfDNA derived from liquid biopsies taken from a cancer-positive and healthy control patient, respectively, are shown in Fig. 6. The detected epialleles for each locus and sample were first visualized by stratifying their respective methylation density into the following bins: unmethylated molecules (<25% methylation), low methylation (25 to 50% methylation density), medium methylation (50 to 75% density), and high methylation (75 to 100% density) based on the corresponding melt temperature of the amplicons (Fig. 6B). The REM-DREAMing platform provided absolute quantification of heterogeneously methylated epialleles in both healthy controls and NSCLC cases for all five biomarkers in the panel (Fig. 7A and fig. S7).

To analyze the resulting data, we adapted and expanded upon a previously developed bioinformatic tool called EpiClass (Epiallelic Methylation Classifier) that uses single-molecule methylation data to identify precise thresholds for methylation density and epiallelic read counts to maximize performance for cancer diagnostic applications (*54*). Here, we sought to use EpiClass to investigate whether the richness of (multiplex) REM-DREAMing data and quantitative single-molecule methylation density analysis could improve the overall diagnostic performance of methylation biomarkers in comparison to traditional methods that rely on predefined methylation patterns (e.g., MSP). We first classified each detected epiallele based on its methylation density into five-percentile bins (0, 5, 10, …, 100%) and subsequently constructed a methylation density histogram for each target locus in the biomarker panel (*54*). We then explored the impact of using different methylation density thresholds on the diagnostic performance of each biomarker by comparing the number of epiallelic molecules with methylation densities over the threshold value in each sample locus; for example, a 30% methylation density threshold identifies the number of molecules that exhibited epiallelic methylation patterns with methylation densities of at least 30%, up to 100%. The AUC was then computed for all samples at each methylation density threshold by comparing the number of hypermethylated read counts for each locus in patients with and without NSCLC (Fig. 7B and fig. S7). For each locus, we also calculated the clinical sensitivity and specificity of each biomarker using the threshold that maximized the difference between the true-positive and

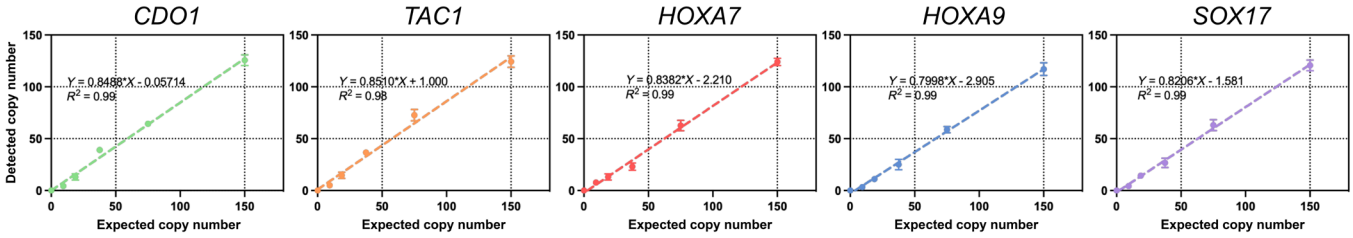

Fig. 5. REM-DREAMing detected versus expected DNA copy number. Synthetic DNA equivalents to the converted *CDO1*, *TAC1*, *HOXA7*, *HOXA9*, and *SOX17* loci ranging in copy numbers of 0, 9.375, 18.75, 37.5, 75, or 150 are mixed with 150 unmethylated background molecules. Each experiment was performed in triplicate to test the reproducibility of each assay.

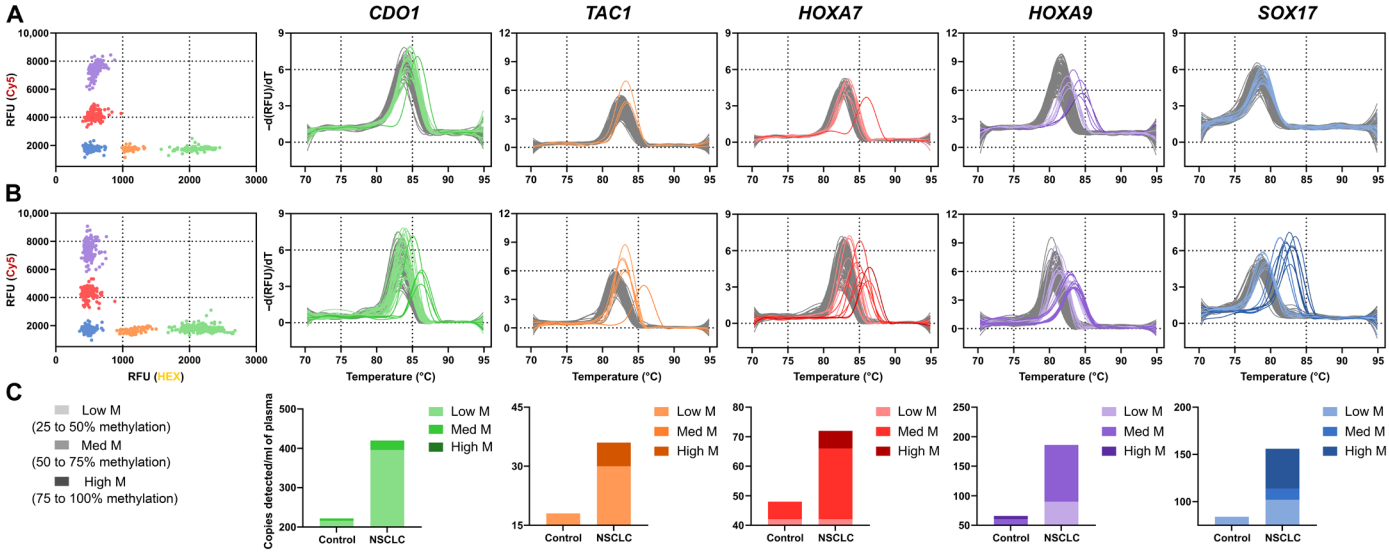

Fig. 6. Representative cfDNA analysis by REM-DREAMing. Results of a CT-positive healthy control (**A**) and an early-stage NSCLC (**B**) are shown here as examples. Fluorescence signal intensity plots are color coded into five populations representing five targets, *CDO1* (green), *TAC1* (orange), *HOXA7* (red), *HOXA9* (purple), and *SOX17* (blue). (A) dHRM curves. All melt derivative curves are color coded into unmethylated (in gray color) or heterogeneously methylated. (**C**) REM-DREAMing analysis visualization histograms.

false-negative rates (fig. S7 and table S3). For *CDO1*, *HOXA7*, and *SOX17*, an intermediate-level methylation threshold (45%, 60%, and 45%) resulted in the highest AUC. In contrast, the optimal methylation density threshold for the *HOXA9* locus was determined to be 90%, indicating epigenetic drift at this locus in otherwise healthy individuals (*55*). Consistent with this interpretation, *HOXA9* also demonstrated the lowest AUC among all five biomarkers.

We next used a multivariate logistic regression model to assess the performance of the biomarker panel in combination. This model was used to determine the optimal methylation density thresholds for each respective biomarker that would achieve the highest AUC for the panel as a whole based on leave-one-out cross-validation. Overall, the results of the multivariate model substantially outperformed any of the individual markers, achieving a clinical sensitivity of 93% at 90% clinical specificity for an overall AUC of 0.96 (95% CI, 0.91 to 1) (Fig. 8 and tables S4 and S5). Notably, the methylation density cutoffs that optimized the panel AUC for *CDO1*, *TAC1*, *HOXA7*, and *SOX17* were identical to those found previously for each individual marker. However, the optimal methylation density threshold for *HOXA9* in combination now shifted from heavy methylation (90%) to intermediate methylation (50%). Overall, for this pilot cohort, the five-plex REM-DREAMing platform substantially outperformed the previously published diagnostic performance for these markers based on combined single-plex MSP (AUC 0.77, 95% CI, 0.68 to 0.86) (*17*), as well as multiplex digital MSP (mdMSP) (AUC 0.86, 95% CI, 0.77 to 0.96) (*56*). To address the imbalance in the number of case and control samples, a precision-recall curve, shown in fig. S9, was also constructed, demonstrating high precision and recall with an AUC of 0.97 (95% CI, 0.92 to 1). Taken as a whole, these results strongly suggest that consideration of intercellular epigenetic heterogeneity can substantially improve the performance of methylation biomarkers for the detection of early-stage cancers.

DISCUSSION

The implementation of dPCR- or NGS-based methods for detecting heterogeneously methylated epialleles in early-stage screening and diagnosis has been historically impeded by technical challenges in analyzing multiple methylation biomarkers in parallel at high sensitivity while also remaining cost-effective. These methods have typically required high volumes of liquid biopsies such as 20 ml of plasma, limiting their practicality for routine use. Previous studies

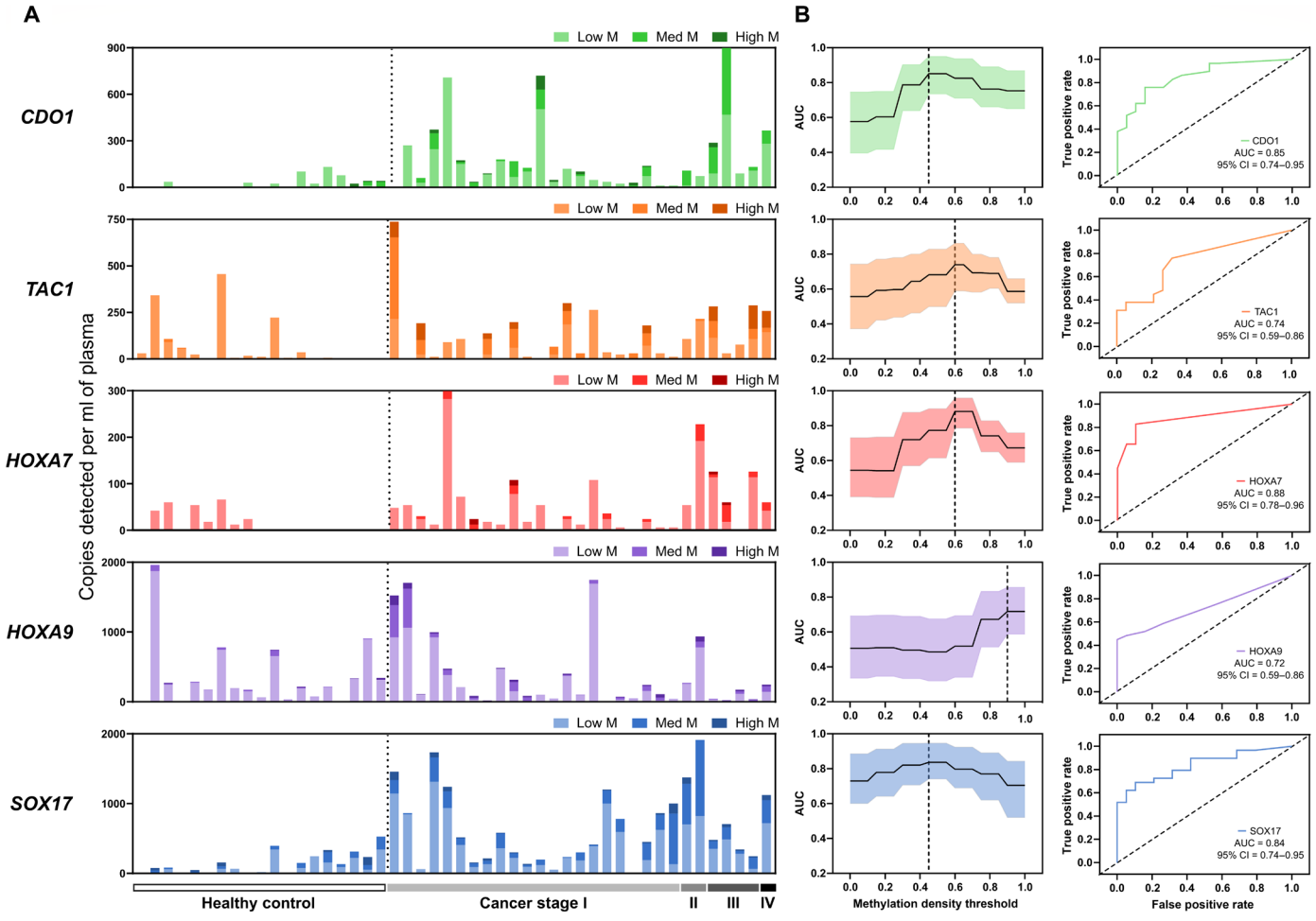

Fig. 7. Diagnostic performance of individual biomarkers. (**A**) Quantitative methylation detection in plasma. Five-plex REM-DREAMing detection of *CDO1*, *TAC1*, *HOXA7*, *HOXA9*, and *SOX17* in plasma samples from 48 patients with CT scan–identified pulmonary nodules. For each locus, the detected epialleles were binned by methylation density (Unmethylated, Low M, Med M, and High M). The full profile is shown in fig. S7. Only Low M, Med M, and High M are shown here for a better visualization. (**B**) Performance of each biomarker across methylation density thresholds. AUC optimized for each locus based on the different methylation density cutoff is listed on the left, and ROC curve with the highest AUC for each locus is shown on the right (with 95% confidence interval labeled in color).

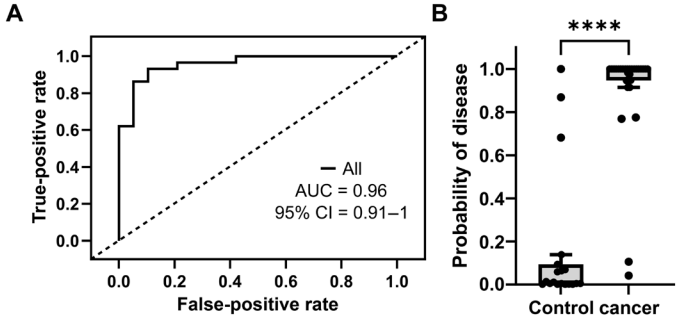

Fig. 8. ROC performance for the detection of NSCLC from REM-DREAMing in plasma. (**A**) ROC curve showing the diagnostic performance of five-plex REM-DREAMing of *CDO1*, *TAC1*, *HOXA7*, *HOXA9*, and *TAC1* methylation in cfDNA from 300 μl of plasma of patients. (**B**) Probability of disease based on the binomial regression model fit. ****$P < 0.0001$ on Wilcoxon rank sum test.

exploring the utility of HRM methods for analyzing heterogeneous methylation patterns projected that the expansion of dPCR methods would greatly facilitate the ability to leverage heterogeneous methylation data to improve the performance and utility of DNA methylation-based biomarkers (*39*, *57*). While numerous digital technologies are now commercially available, to the best of our knowledge, there currently does not exist a commercial technology that offers users the ability to perform parallelized dHRM. Here, we presented an innovative, low-cost method called REM-DREAMing that leverages digital microfluidics with a ratiometric fluorescence detection scheme and precise dHRM analysis to enable parallelized analysis of intermolecular epigenetic heterogeneity of methylation biomarker panels at single-copy sensitivity (table S7).

Liquid biopsies have engendered substantial interest as a promising approach for the detection of a myriad of cancer types, including NSCLC. NSCLC accounts for 85% of all lung cancer cases and has a 5-year survival rate of only 25% (*58*). While low-dose CT screening has led to a 20% reduction in lung cancer mortality, it is nonetheless plagued by a high false-positive rate, leading to overdiagnosis, as well as substantial patient risk associated with follow-up procedures (*58*–*64*). Consequently, there has been considerable interest in the development of complementary screening approaches that might supplement low-dose CT screening tests by providing

additional information that can help to reduce false positives and improve the accuracy of NSCLC detection. Toward this end, in our prior work, we identified a panel of five epigenetic biomarkers, *CDO1*, *TAC1*, *HOXA7*, *HOXA9*, and *SOX17*, which are commonly hypermethylated in NSCLC and demonstrated that cancer-specific aberrant methylation can be detected in noninvasively collected liquid biopsies from patients with cancer using traditional approaches [i.e., quantitative methylation-specific PCR (qMSP)] (*17*, *50*). While cancer-specific methylation can be detected in plasma using traditional PCR-based approaches, current methods are fundamentally limited by an inability to detect heterogeneous methylation patterns. Likewise, a key goal of the present study was to determine whether digital high-resolution epiallelic analysis (by REM-DREAMing) could address this barrier to further improve the clinical performance of these biomarkers. To test this hypothesis, we developed an analogous, multiplex DREAMing assay for this five-biomarker panel as a model system to determine whether the superior analytical performance of REM-DREAMing would translate into improved clinical performance for early-stage cancer detection. Toward this end, a key advantage of the REM-DREAMing platform over traditional MSP-based approaches is the resulting richness of data that provides a comprehensive assessment of epiallelic distributions of biomarkers or loci of interest in a given panel. More specifically, DREAMing provides copy-by-copy analysis of methylation density that can better resolve subtle statistical differences in the epiallelic distributions of healthy versus cancerous tissues, which can then be leveraged to improve clinical sensitivity while maintaining appropriate specificity. Our results demonstrate that assessing methylation density at the level of individual DNA molecules can help establish effective thresholds capable of overcoming noise arising from various background sources such as biological or technical variation and age-related epigenetic drift. Using data from REM-DREAMing analysis, we were able to demonstrate that optimized methylation density thresholding substantially improved clinical sensitivity to 93% at 90% specificity, yielding a corresponding AUC of 0.96 (95% CI, 0.91 to 1), in comparison to previously reported single-plex data, which exhibited a clinical sensitivity of 86% at 78% specificity and an AUC of 0.77 (95% CI, 0.68 to 0.86) (*17*). Another advantage of REM-DREAMing is the ability to obtain enriched datasets for multiple biomarkers in smaller sample volumes (e.g., 1 ml) compared to many NGS-based techniques that can require upward of 5 ml or more per assay. Overall, the results of this study suggest that the five-marker REM-DREAMing assay holds potential to improve outcomes in CT scan–positive patients by substantially reducing unnecessary invasive, and potentially hazardous, follow-up procedures. It also emphasizes the potential clinical utility of improved digital approaches as a strategy to enhance patient outcomes and decrease health care expenses.

While dPCR-based approaches often offer high sensitivity for cancer biomarker detection in liquid biopsies, they are traditionally limited in their ability to achieve higher degrees of multiplexing capability. Most dPCR methods are limited by using one fluorescent channel (one fluorophore-labeled probe) for each target, restricting analysis to no more than four targets per assay (*17*, *19*–*21*, *65*, *66*). This challenge is particularly problematic for HRM and dHRM-based assays due to the need to reserve a fluorescence channel for profiling DNA melting that can only resolve a single melt curve in each reaction volume. The most used commercial digital PCR technologies exhibit several limitations and are currently unsuitable for applications involving digital HRM. For example, while several high-density array-based platforms (e.g., Biomark from Fluidigm, QuantStudio from Thermo Fisher Scientific, and QIAcuity from Qiagen) are commercially available, these universally rely on endpoint measurements and do not support dHRM analysis.

Other complications that commonly plague multiplex PCR assays are issues arising from competitive amplification between targets and nonspecific interactions (e.g., heteroduplexes, primer dimers, etc.). Primer-dimer issues are particularly exacerbated in assays with high multiplexing orders as the number of potential primer-primer interactions for an n-plex assay is equal to $2n^2 + n$ (*67*). Overcoming this problem can be a tedious and intricate process, often requiring multiple rounds of design modifications that may alter the target loci and compromise the analytical and diagnostic performance of the assay. To address these challenges, we adopted a multiplex primer design bioinformatic pipeline designed to identify groups of primer sequences that exhibit minimal interprimer interactions. As discussed in our prior work (*38*), nonspecific interactions are sometimes observable in the resulting melt profiles; however, these interactions are uncommon and have negligible effect on REM-DREAMing assay because they produce minor secondary melt peaks that lie below the amplicon T_m range.

While REM-DREAMing effectively employs dHRM to assess epiallelic methylation density, one potential limitation is an inability to determine precise epigenetic polymorphisms. While elucidation of precise methylation patterns can be of utility for particular applications, we have found that this information is not essential for maximizing sensitivity for cancer diagnostic and screening applications. In our previous publication, EpiClass, we conducted a comparison of diagnostic performance between DREAMing and other methods that use epigenetic polymorphisms for cancer detection. In short, we demonstrated that by using EpiClass to optimize methylation density thresholds, our method is able to reliably outperform assays based on methylation haplotypes (*54*). While our technique is not designed for detecting epi-polymorphism directly, it can identify clinical samples that are meaningful for further investigation into epi-polymorphism to uncover underlying biological implications.

There are also a few limitations in the current platform that need refinement for better clinical applicability. The present chip has a restricted number of nanowells per module that constrains the dynamic range for DNA measurements, particularly for multiplex digital assays that require all targets to be digitized into independent nanowells. While multiple modules can in principle be used to achieve higher digitization power for samples with high DNA quantities, this approach would compromise overall sample throughput. These challenges could be overcome by enhancing the nanowell density (*68*) or by incorporating more modules into an expanded device. These amendments will require incorporation of improved optical instrumentation with higher resolution and sensitivity in next-generation devices. Last, the statistical power of our study was constrained by a cohort size of 48 specimens, and the retrospective design might be susceptible to selection bias. Follow-up studies will require validation in a larger, prospectively collected cohort to reduce overfitting and more comprehensively assess clinical performance.

In conclusion, we showed that REM-DREAMing provides a simple, low-cost means of comprehensively profiling intermolecular methylation heterogeneity in extended panels of methylation biomarkers by providing simultaneous assessment of epiallelic methylation patterns at

single-copy sensitivity. This approach presents a few technical advantages over other existing methylation diagnostic approaches (see table S7), particularly in terms of sensitivity, resolution, and multiplexing capability, while substantially reducing time and cost in comparison to NGS-based assays. Our work underscores the importance of further biological studies to explore the biological implications of methylation density and epigenetic heterogeneity more deeply, particularly in the context of carcinogenesis and cancer biology. Overall, REM-DREAMing offers a solution for assessing epigenetic heterogeneity of biomarker panels for numerous diagnostic applications, with the potential to serve as a routine screening tool for early-stage cancer detection.

MATERIALS AND METHODS

Primer and probe selection

A methylation-independent primer design was used by adapting our previously published design criteria and an online tool PrimerSuite (*38*, *69*) (fig. S5). Briefly, the design rules were as follows: (i) inclusion of no more than two CpG sites in each primer toward the 5′ end of the primer; (ii) amplicon size preferentially shorter than 150 bp; (iii) primer melting temperatures near 60°C and within 2°C of each other; (iv) specificity check by BiSearch toward both bisulfite converted and genomic DNA (*70*); (v) no or minimized primer-dimer formation; (vi) single-peak melt profiles for both fully methylated and fully unmethylated BST sequences, as determined by uMELT Quartz and bulk experiments (fig. S10) (*71*); and (vii) at least seven CpG sites in the internal region between primers as the melting temperature difference between fully unmethylated and fully methylated DNA is generally proportional to the number of CpG sites. Forward-reverse primer pairs that met the above criteria were added to a candidate DREAMing primer pool for in silico assessment of nonspecific interactions between all candidate primers. Primer pairs with no predicted primer-dimer formation or primer dimers with a ΔG higher than −1 are added into the final REM-DREAMing primer pool (*69*). Probe design follows general TaqMan probe design rules. Briefly, no more than two CpG dinucleotides could be present in the probe sequences. Melting temperatures are at least 4°C higher than those of the corresponding primers (higher is generally better). All primers and probes were ordered from Integrated DNA Technologies (IDT).

Microfluidic device fabrication

Microfluidic devices were fabricated using standard photolithography and soft lithography techniques. Photomasks were designed using AutoCAD software and printed by Artnet Pro. The reusable master molds were fabricated using SU-8 3025 and SU-8 3050 photoresists (MicroChem) to create multilayer patterns on a 4-inch silicon wafer. SU-8 3025 was spun on a dehydrated silicon wafer at 2000 rpm for 30 s. After soft baking at 65°C for 5 min and 95°C for 30 min, the wafer was exposed at 200 mJ/cm^2 and developed to define microchannel patterns. After a hard bake at 200°C for 2 hours, SU-8 3050 was spun on top of the microchannel layer at 1000 rpm for 30 s. The wafer was then soft baked at 65°C for 15 min and at 95°C for 1 hour. Last, the wafer was exposed at 320 mJ/cm^2, developed, and baked at 200°C for 2 hours to define the resulting nanowell pattern.

Each microfluidic device was fabricated from this mold using our previously published ultrathin soft lithography technique (*39*, *56*). Briefly, the wafer was treated with chlorotrimethylsilane (Sigma-Aldrich) in a vacuum chamber for 2 min to increase the hydrophobicity of the silicon wafer surface. A 10:1 mixture of PDMS from SYLGARD 184 Silicone Elastomer Kit (Dow Chemical Company) was spun on the wafer surface at 400 rpm and spun on a blank wafer at 100 rpm as a sacrificial layer. Both were baked for 5 min at 80°C. The sacrificial layer was then peeled off and overlaid on the top of the pattern surface and baked for 6 min at 80°C. The two partially bonded PDMS layers on the pattern layer were peeled off together. A large microscope glass slide (75 mm by 50 mm by 1 mm thick; Ted Pella) was cleaned and air-dried. A 10:1 mixture of PDMS was spun on the glass slide at 2100 rpm and then baked at 80°C for 6 min. The patterned-sacrificial-jointed layer and PDMS-covered glass slide were oxygen plasma treated at 40 to 45 W for 45 s and then bonded. After bonding, the sacrificial layer was removed. Subsequently, a thin cover glass slide and tubing adapter layer were oxygen plasma bonded to the top surface. The fabricated devices were baked at 80°C overnight, sealed with a piece of thin adhesive tape (Scotch), and desiccated for at least 3 hours.

Sample loading and digitization

Each dPCR master mix contains 28 μl of PCR mixture consisting of 16.6 mM $(NH_4)_2SO_4$, 67 mM tris (pH 8.8), 2.7 mM $MgCl_2$, 10 mM β-mercaptoethanol, 200 nM primers (IDT), 200 μM each deoxynucleotide triphosphate (dNTP, MilliporeSigma), Platinum Taq DNA polymerase (0.07 U/μl; Thermo Fisher Scientific), bovine serum albumin (1 mg/ml; New England BioLabs), 0.01% Tween 20 (Sigma-Aldrich), and 1× EvaGreen Plus (Biotium). Cy5- and HEX-labeled TaqMan probes specific to each biomarker were added based on the predefined concentration ratios with a total concentration of 0.16 μM. For clinical sample tests, 5 μl of bisulfite converted DNA sample was used. Sample loading for digitization was conducted based on the previously described approach (*39*, *56*). Briefly, a 1-ml syringe (BD Syringe) storing PCR master mix was used to puncture the sealed inlet of a microfluidic device. The negative pressure difference present in the sealed microfluidic device due to desiccation affects sample loading. Partitioning fluid was prepared by mixing 5 g of silicon oil and 1 g of a 10:1 mixture of PDMS and was then drawn into microcentrifuge tubing (Cole-Parmer). Partitioning oil was pressurized into the channels of a microfluidic chip to digitize the 10,400 wells of each module. All synthetic control DNA was also purchased from IDT and used based on the concentration provided by the manufacturer.

Digital PCR and image acquisition

The microfluidic chip was placed on a flatbed thermal cycler (Bulldog Bio) with partitioning fluid pressurized to 11 psi at one end and sealed at the other end. Thermal conductivity was enhanced by having FC 40 (Sigma-Aldrich) between the glass slide and the heating block. The dPCR cycling conditions were 95°C for 5 min and 70 cycles of 95°C for 30 s, 58°C for 30 s, and 72°C for 30 s. Because of the addition of PDMS, the partitioning fluid solidified during thermocycling to provide barriers between channels and nanowells to digitize the sample and prevent cross-contamination between nanowells during PCR and subsequent analyses. Following the completion of PCR, the microfluidic device was detached from the pressure regulator and removed from the thermal cycler. The microfluidic device was then scanned with an Amersham Typhoon 5 Biomolecular Imager (GE Healthcare) equipped with lasers with excitation wavelengths of 488, 532, and 635 nm and accompanying filters for emission wavelengths ranging from 515 to 685 nm to obtain the whole-field fluorescence images for EvaGreen, HEX, and Cy5-labeled probes. To conduct digital melt, the chip was placed on a flatbed heater (Bulldog Bio) and

illuminated by a blue light-emitting diode (LED) array (Thorlabs). The wide field-of-view images were captured by a Sony Alpha 7 III with a Sony FE 50-mm F2.8 Macro lens, which was coupled to a green filter (Omega Optical). The temperature of the heater ramped at a rate of 0.1°C/s from 70 to 95°C. Images were captured at 1 Hz with a 0.6-s exposure time. The principles for distinguishing various methylation patterns using dHRM analysis have been described previously (*39*). Briefly, after dPCR, methylation density profiling of amplified amplicons in positive wells relies on measuring the temperature-dependent release of dsDNA binding dye due to amplicon denaturation during thermal ramping. Fluorescence images of the chip area are captured simultaneously during temperature ramping to record the denaturation of each digitized target. The fluorescence signal is then extracted and filtered to produce a melt curve for each amplicon in every positive nanowell. The peak in the negative derivative of the melt curve (T_m) corresponds to the methylation density of the original template molecules at the target loci.

Imaging processing

Image processing was conducted using a custom-developed program written in MATLAB as previously described (*39*, *56*). In short, four corner points of the array were selected and a script generates a linearly scaled mask of the array. To address any misalignment, a homography transformation was applied to the array mask using the four user-selected points and the generated corners. Empty spaces or dark strips among nanowell columns and rows were used as features to further correct misalignment if present. The well boundaries were cropped by 20% on each side so that only the central mass of the mixture was used for the measurement of Cy5 or HEX fluorescence intensity. Positive wells were determined by the presence of EvaGreen-positive signals and peaks in the negative derivative of the melt curves. Biomarker identification was achieved using a threshold based on ~95% CIs for each ratiometric fluorescence signature (fig. S1). The EvaGreen fluorescence intensity values within each nanowell were averaged in temperature intervals of 0.3°C. Low-pass and Savitzky-Golay filters were applied to generate smoothed melt curves. The melt temperature of each amplicon was identified as the peak of the negative derivative of the signal as a function of temperature.

Sample population and plasma extraction

The study population comprised a prospective, observational cohort, initiated in 1996 within the University of Pittsburgh ("Detection of Genetic Markers of Lung Cancer Initiation and Progression," IRB no. 19,060,269). All patients provided informed consent. Patients had a CT scan due to the suspicion of lung cancer and were subsequently referred to surgery for resection. Surgical resection with curative intent and pathological analyses of suspected lung cancer lesions were completed in all patients and staged according to revised TNM Classification of Malignant Tumors (TNM) guideline classification criteria (*71*). Cases had pathologically confirmed NSCLC and controls were pathologically confirmed to have a benign condition. Pack-years of cigarette smoking were defined as the average number of packs smoked per day times the number of years smoked. Plasma samples were collected in tubes containing sodium heparin (Becton, Dickinson and Company) and then stored at −80°C until use.

DNA extraction and bisulfite conversion

DNA extraction from plasma was performed with the NeoGeneStar Circulating DNA Purification Kit (NeoGeneStar) according to the manufacturer's protocol. Briefly, 1.0 to 2.0 ml of plasma was digested in a solution containing Protease Buffer and 1× Proteinase K (New England Biolabs) for 30 min at 55 to 60°C. DNA was then precipitated by isopropanol, washed by a series of decantation steps, and eluted into 30 μl of elution buffer. Long interspersed nuclear element 1 (LINE-1) standards were used to estimate the overall cfDNA copy numbers with 300 nM forward primer, 5′-AGG GTT TTT ATG GTT TTA GGT T-3′, 300 nM reverse primer, 5′-ATC CCT TCC TTA CAC C-3′, spanning 82-bp regions, and 100 nM probe, 5′-\6FAM\TTG AAT TGA TTT TGT ATA A\MGBNFQ\-3′. Cycling conditions were 95°C for 5 min, and 50 cycles of 95°C for 30 s, 50°C for 30 s, and 72°C for 30 s. PCR was conducted using a PCR buffer containing 16.6 mM $(NH_4)_2SO_4$, 67 mM tris (pH 8.8), 10 mM β-mercaptoethanol, and magnesium chloride to yield a final magnesium concentration of 6.7 mM, 200 μM dNTP (MilliporeSigma), and 0.04 U μl^{-1} of Platinum *Taq* polymerase (Thermo Fisher Scientific). Final reaction volumes for LINE-1 quantification assays were 25 μl. The resulting DNA was bisulfite treated using the EZ DNA Methylation-Lightning Kit (ZYMO RESEARCH) according to the manufacturer's instructions and eluted into a final volume of 30 μl. The yields of the BST cfDNA were quantified by LINE-1 quantification assay as described above.

Univariate and multivariate analysis

The method used to determine the optimal methylation density cutoff for each individual biomarker follows our previously published Epiallelic Methylation Classifier (EpiClass) pipeline (*54*). Briefly, a range of values for methylation density (0, 5, 10, …, 100%) was tested for each respective biomarker, with a range of methylated epiallele counts to determine the optimal methylation density and count cutoff. The sensitivity + specificity or, equivalently, true-positive rate (TPR) − false-positive rate (FPR) is calculated and the maximum is used to determine the optimal cutoff. In the multivariate analysis, a logistic regression was used to construct a predictive model for cancer status based on the DNA methylation levels of any marker panel combination. The full model of multivariate analysis is shown in table S4. To minimize the impact of overfitting, the evaluation of performance was conducted through the use of a leave-one-out cross-validation design. The input entering the ROC curve computation was the probability, predicted for each observation validation sample. This probability determined whether the observation would be categorized into the case or control class, as assigned by the algorithm. These probabilities were used as classification thresholds to identify the number of true and false positives and negatives and are further converted to true-positive rate and false-positive rate. The resulting metrics were subsequently used to construct the ROC curves. The performance was assessed by an AUC and reported with its accompanying bootstrap-derived 95% CIs. All analyses were performed using the R statistical software suite, accessible at http://r-project.org, with both standard software packages and custom code implementations.

Supplementary Materials

This PDF file includes:

Figs. S1 to S10
Tables S1 to S7

REFERENCES AND NOTES

1. A. L. Mattei, N. Bailly, A. Meissner, DNA methylation: A historical perspective. *Trends Genet.* **38**, 676–707 (2022).
2. S. B. Baylin, J. G. Herman, DNA hypermethylation in tumorigenesis: Epigenetics joins genetics. *Trends Genet.* **16**, 168–174 (2000).

3. H. Easwaran, H. C. Tsai, S. B. Baylin, Cancer epigenetics: Tumor heterogeneity, plasticity of stem-like states, and drug resistance. *Mol. Cell* **54**, 716–727 (2014).
4. D. Sidransky, Emerging molecular markers of cancer. *Nat. Rev. Cancer* **2**, 210–219 (2002).
5. T. R. Pisanic II, P. Athamanolap, T. H. Wang, Defining, distinguishing and detecting the contribution of heterogeneous methylation to cancer heterogeneity. *Semin. Cell Dev. Biol.* **64**, 5–17 (2017).
6. G. Landan, N. M. Cohen, Z. Mukamel, A. Bar, A. Molchadsky, R. Brosh, S. Horn-Saban, D. A. Zalcenstein, N. Goldfinger, A. Zundelevich, E. N. Gal-Yam, V. Rotter, A. Tanay, Epigenetic polymorphism and the stochastic formation of differentially methylated regions in normal and cancerous tissues. *Nat. Genet.* **44**, 1207–1214 (2012).
7. M. Guo, Y. Peng, A. Gao, C. Du, J. G. Herman, Epigenetic heterogeneity in cancer. *Biomark Res.* **7**, 23 (2019).
8. D. Brocks, Y. Assenov, S. Minner, O. Bogatyrova, R. Simon, C. Koop, C. Oakes, M. Zucknick, D. B. Lipka, J. Weischenfeldt, L. Feuerbach, R. C.-S. Lari, M. Lupien, B. Brors, J. Korbel, T. Schlomm, A. Tanay, G. Sauter, C. Gerhäuser, C. Plass; ICGC Early Onset Prostate Cancer Project, Intratumor DNA methylation heterogeneity reflects clonal evolution in aggressive prostate cancer. *Cell Rep.* **8**, 798–806 (2014).
9. S. C. Zheng, M. Widschwendter, A. E. Teschendorff, Epigenetic drift, epigenetic clocks and cancer risk. *Epigenomics* **8**, 705–719 (2016).
10. G. Russo, A. Tramontano, I. Iodice, L. Chiariotti, A. Pezone, Epigenome chaos: Stochastic and deterministic DNA methylation events drive cancer evolution. *Cancer* **13**, 1800 (2021).
11. H. Schwarzenbach, D. S. Hoon, K. Pantel, Cell-free nucleic acids as biomarkers in cancer patients. *Nat. Rev. Cancer* **11**, 426–437 (2011).
12. C. Bettegowda, M. Sausen, R. J. Leary, I. Kinde, Y. Wang, N. Agrawal, B. R. Bartlett, H. Wang, B. Luber, R. M. Alani, E. S. Antonarakis, N. S. Azad, A. Bardelli, H. Brem, J. L. Cameron, C. C. Lee, L. A. Fecher, G. L. Gallia, P. Gibbs, D. Le, R. L. Giuntoli, M. Goggins, M. D. Hogarty, M. Holdhoff, S.-M. Hong, Y. Jiao, H. H. Juhl, J. J. Kim, G. Siravegna, D. A. Laheru, C. Lauricella, M. Lim, E. J. Lipson, S. K. N. Marie, G. J. Netto, K. S. Oliner, A. Olivi, L. Olsson, G. J. Riggins, A. Sartore-Bianchi, K. Schmidt, I.-M. Shih, S. M. Oba-Shinjo, S. Siena, D. Theodorescu, J. Tie, T. T. Harkins, S. Veronese, T.-L. Wang, J. D. Weingart, C. L. Wolfgang, L. D. Wood, D. Xing, R. H. Hruban, J. Wu, P. J. Allen, C. M. Schmidt, M. A. Choti, V. E. Velculescu, K. W. Kinzler, B. Vogelstein, N. Papadopoulos, L. A. Diaz Jr., Detection of circulating tumor DNA in early- and late-stage human malignancies. *Sci. Transl. Med.* **6**, 224ra224 (2014).
13. I. Amelio, R. Bertolo, P. Bove, O. C. Buonomo, E. Candi, M. Chiocchi, C. Cipriani, N. Di Daniele, C. Ganini, H. Juhl, A. Mauriello, C. Marani, J. Marshall, M. Montanaro, G. Palmieri, M. Piacentini, G. Sica, M. Tesauro, V. Rovella, G. Tisone, Y. Shi, Y. Wang, G. Melino, Liquid biopsies and cancer omics. *Cell Death Discov.* **6**, 131 (2020).
14. A. P. Feinberg, R. Ohlsson, S. Henikoff, The epigenetic progenitor origin of human cancer. *Nat. Rev. Genet.* **7**, 21–33 (2006).
15. K. Cibulskis, M. S. Lawrence, S. L. Carter, A. Sivachenko, D. Jaffe, C. Sougnez, S. Gabriel, M. Meyerson, E. S. Lander, G. Getz, Sensitive detection of somatic point mutations in impure and heterogeneous cancer samples. *Nat. Biotechnol.* **31**, 213–219 (2013).
16. C. Fiala, E. P. Diamandis, New approaches for detecting cancer with circulating cell-free DNA. *BMC Med.* **17**, 159 (2019).
17. A. Hulbert, I. Jusue-Torres, A. Stark, C. Chen, K. Rodgers, B. Lee, C. Griffin, A. Yang, P. Huang, J. Wrangle, S. A. Belinsky, T. H. Wang, S. C. Yang, S. B. Baylin, M. V. Brock, J. G. Herman, Early detection of lung cancer using DNA promoter hypermethylation in plasma and sputum. *Clin. Cancer Res.* **23**, 1998–2005 (2017).
18. B. Liu, J. Ricarte Filho, A. Mallisetty, C. Villani, A. Kottorou, K. Rodgers, C. Chen, T. Ito, K. Holmes, N. Gastala, K. Valyi-Nagy, O. David, R. C. Gaba, C. Ascoli, M. Pasquinelli, L. E. Feldman, M. G. Massad, T. H. Wang, I. Jusue-Torres, E. Benedetti, R. A. Winn, M. V. Brock, J. G. Herman, A. Hulbert, Detection of promoter DNA methylation in urine and plasma aids the detection of non-small cell lung cancer. *Clin. Cancer Res.* **26**, 4339–4348 (2020).
19. C. A. Eads, K. D. Danenberg, K. Kawakami, L. B. Saltz, C. Blake, D. Shibata, P. V. Danenberg, P. W. Laird, MethyLight: A high-throughput assay to measure DNA methylation. *Nucleic Acids Res.* **28**, E32 (2000).
20. Y. M. Lo, I. H. Wong, J. Zhang, M. S. Tein, M. H. Ng, N. M. Hjelm, Quantitative analysis of aberrant p16 methylation using real-time quantitative methylation-specific polymerase chain reaction. *Cancer Res.* **59**, 3899–3903 (1999).
21. B. N. Trinh, T. I. Long, P. W. Laird, DNA methylation analysis by MethyLight technology. *Methods* **25**, 456–462 (2001).
22. M. Yu, K. T. Carter, K. W. Makar, K. Vickers, C. M. Ulrich, R. E. Schoen, D. Brenner, S. D. Markowitz, W. M. Grady, MethyLight droplet digital PCR for detection and absolute quantification of infrequently methylated alleles. *Epigenetics* **10**, 803–809 (2015).
23. M. I. Husseiny, A. Fahmy, W. Du, A. Gu, P. Garcia, K. Ferreri, F. Kandeel, Development of quantitative methylation-specific droplet digital PCR (ddMSP) for assessment of natural Tregs. *Front. Genet.* **11**, 300 (2020).
24. N. Uehiro, F. Sato, F. Pu, S. Tanaka, M. Kawashima, K. Kawaguchi, M. Sugimoto, S. Saji, M. Toi, Circulating cell-free DNA-based epigenetic assay can detect early breast cancer. *Breast Cancer Res.* **18**, 129 (2016).
25. T. Hata, M. Dal Molin, S. M. Hong, K. Tamura, M. Suenaga, J. Yu, H. Sedogawa, M. J. Weiss, C. L. Wolfgang, A. M. Lennon, R. H. Hruban, M. G. Goggins, Predicting the grade of dysplasia of pancreatic cystic neoplasms using cyst fluid DNA methylation markers. *Clin. Cancer Res.* **23**, 3935–3944 (2017).
26. K. H. Taylor, R. S. Kramer, J. W. Davis, J. Guo, D. J. Duff, D. Xu, C. W. Caldwell, H. Shi, Ultradeep bisulfite sequencing analysis of DNA methylation patterns in multiple gene promoters by 454 sequencing. *Cancer Res.* **67**, 8511–8518 (2007).
27. A. Meissner, A. Gnirke, G. W. Bell, B. Ramsahoye, E. S. Lander, R. Jaenisch, Reduced representation bisulfite sequencing for comparative high-resolution DNA methylation analysis. *Nucleic Acids Res.* **33**, 5868–5877 (2005).
28. M. Bibikova, Z. Lin, L. Zhou, E. Chudin, E. W. Garcia, B. Wu, D. Doucet, N. J. Thomas, Y. Wang, E. Vollmer, T. Goldmann, C. Seifart, W. Jiang, D. L. Barker, M. S. Chee, J. Floros, J. B. Fan, High-throughput DNA methylation profiling using universal bead arrays. *Genome Res.* **16**, 383–393 (2006).
29. J. Phallen, M. Sausen, V. Adleff, A. Leal, C. Hruban, J. White, V. Anagnostou, J. Fiksel, S. Cristiano, E. Papp, S. Speir, T. Reinert, M. W. Orntoft, B. D. Woodward, D. Murphy, S. Parpart-Li, D. Riley, M. Nesselbush, N. Sengamalay, A. Georgiadis, Q. K. Li, M. R. Madsen, F. V. Mortensen, J. Huiskens, C. Punt, N. van Grieken, R. Fijneman, G. Meijer, H. Husain, R. B. Scharpf, L. A. Diaz Jr., S. Jones, S. Angiuoli, T. Orntoft, H. J. Nielsen, C. L. Andersen, V. E. Velculescu, Direct detection of early-stage cancers using circulating tumor DNA. *Sci. Transl. Med.* **9**, eaan2415 (2017).
30. T. Mikeska, I. L. Candiloro, A. Dobrovic, The implications of heterogeneous DNA methylation for the accurate quantification of methylation. *Epigenomics* **2**, 561–573 (2010).
31. P. W. Laird, Principles and challenges of genomewide DNA methylation analysis. *Nat. Rev. Genet.* **11**, 191–203 (2010).
32. A. M. Newman, S. V. Bratman, J. To, J. F. Wynne, N. C. Eclov, L. A. Modlin, C. L. Liu, J. W. Neal, H. A. Wakelee, R. E. Merritt, J. B. Shrager, B. W. Loo Jr., A. A. Alizadeh, M. Diehn, An ultrasensitive method for quantitating circulating tumor DNA with broad patient coverage. *Nat. Med.* **20**, 548–554 (2014).
33. S. Y. Shen, R. Singhania, G. Fehringer, A. Chakravarthy, M. H. A. Roehrl, D. Chadwick, P. C. Zuzarte, A. Borgida, T. T. Wang, T. Li, O. Kis, Z. Zhao, A. Spreafico, T. D. S. Medina, Y. Wang, D. Roulois, I. Ettayebi, Z. Chen, S. Chow, T. Murphy, A. Arruda, G. M. O'Kane, J. Liu, M. Mansour, J. D. McPherson, C. O'Brien, N. Leighl, P. L. Bedard, N. Fleshner, G. Liu, M. D. Minden, S. Gallinger, A. Goldenberg, T. J. Pugh, M. M. Hoffman, S. V. Bratman, R. J. Hung, D. D. De Carvalho, Sensitive tumour detection and classification using plasma cell-free DNA methylomes. *Nature* **563**, 579–583 (2018).
34. M. C. Liu, G. R. Oxnard, E. A. Klein, C. Swanton, M. V. Seiden; CCGA Consortium, Sensitive and specific multi-cancer detection and localization using methylation signatures in cell-free DNA. *Ann. Oncol.* **31**, 745–759 (2020).
35. F. Zhao, B. Bapat, The role of methylation-specific PCR and associated techniques in clinical diagnostics. *Epigenetic Biomarkers and Diagnostics*, 155–173 (2016).
36. S. Samso Mathiasen, J. Binkowski, T. Kjeldsen, T. K. Wojdacz, L. L. Hansen, Methylation levels assessment with methylation-sensitive high-resolution melting (MS-HRM). *PLOS ONE* **17**, e0273058 (2022).
37. E. Khodadadi, L. Fahmideh, E. Khodadadi, S. Dao, M. Yousefi, S. Taghizadeh, M. Asgharzadeh, B. Yousefi, H. S. Kafil, Current advances in DNA methylation analysis methods. *Biomed. Res. Int.* **2021**, 8827516 (2021).
38. T. R. Pisanic II, P. Athamanolap, W. Poh, C. Chen, A. Hulbert, M. V. Brock, J. G. Herman, T. H. Wang, DREAMing: A simple and ultrasensitive method for assessing intratumor epigenetic heterogeneity directly from liquid biopsies. *Nucleic Acids Res.* **43**, e154 (2015).
39. C. M. O'Keefe, T. R. Pisanic II, H. Zec, M. J. Overman, J. G. Herman, T.-H. Wang, Facile profiling of molecular heterogeneity by microfluidic digital melt. *Sci. Adv.* **4**, eaat6459 (2018).
40. V. J. Bailey, B. P. Keeley, C. R. Razavi, E. Griffiths, H. E. Carraway, T. H. Wang, DNA methylation detection using MS-qFRET, a quantum dot-based nanoassay. *Methods* **52**, 237–241 (2010).
41. B. Keeley, A. Stark, T. R. Pisanic II, R. Kwak, Y. Zhang, J. Wrangle, S. Baylin, J. Herman, N. Ahuja, M. V. Brock, T.-H. Wang, Extraction and processing of circulating DNA from large sample volumes using methylation on beads for the detection of rare epigenetic events. *Clin. Chim. Acta* **425**, 169–175 (2013).
42. V. J. Bailey, Y. Zhang, B. P. Keeley, C. Yin, K. L. Pelosky, M. Brock, S. B. Baylin, J. G. Herman, T. H. Wang, Single-tube analysis of DNA methylation with silica superparamagnetic beads. *Clin. Chem.* **56**, 1022–1025 (2010).
43. P. Yakovchuk, E. Protozanova, M. D. Frank-Kamenetskii, Base-stacking and base-pairing contributions into thermal stability of the DNA double helix. *Nucleic Acids Res.* **34**, 564–574 (2006).
44. R. Netzer, D. Ribicic, M. Aas, L. Cave, T. Dhawan, Absolute quantification of priority bacteria in aquaculture using digital PCR. *J. Microbiol. Methods* **183**, 106171 (2021).
45. Z. Ge, J. C. A. Helmijr, M. Jansen, P. P. C. Boor, L. Noordam, M. Peppelenbosch, J. Kwekkeboom, J. Kraan, D. Sprengers, Detection of oncogenic mutations in paired circulating tumor DNA and circulating tumor cells in patients with hepatocellular carcinoma. *Transl. Oncol.* **14**, 101073 (2021).

46. C. Tumpach, C. R. Cochrane, Y. Kim, J. Ong, A. Rhodes, T. A. Angelovich, M. J. Churchill, S. R. Lewin, S. Telwatte, M. Roche, Adaptation of the intact proviral DNA assay to a nanowell-based digital PCR platform. *J. Virus Erad.* **9**, 100335 (2023).
47. R. C.-W. Wong, A. H. Wong, Y. I. Ho, G. K. Siu, L. K. Lee, E. C. Leung, R. W. Lai, Application of digital PCR to determine the reliability of Xpert Xpress SARS-CoV-2 assay with envelope (E) gene negative and nucleocapsid (N2) gene positive results. *Diagn. Microbiol. Infect. Dis.* **103**, 115726 (2022).
48. J. E. Kreutz, T. Munson, T. Huynh, F. Shen, W. Du, R. F. Ismagilov, Theoretical design and analysis of multivolume digital assays with wide dynamic range validated experimentally with microfluidic digital PCR. *Anal. Chem.* **83**, 8158–8168 (2011).
49. P. L. Quan, M. Sauzade, E. Brouzes, dPCR: A technology review. *Sensors* **18**, (2018).
50. J. Wrangle, E. O. Machida, L. Danilova, A. Hulbert, N. Franco, W. Zhang, S. C. Glockner, M. Tessema, L. Van Neste, H. Easwaran, K. E. Schuebel, J. Licchesi, C. M. Hooker, N. Ahuja, J. Amano, S. A. Belinsky, S. B. Baylin, J. G. Herman, M. V. Brock, Functional identification of cancer-specific methylation of CDO1, HOXA9, and TAC1 for the diagnosis of lung cancer. *Clin. Cancer Res.* **20**, 1856–1864 (2014).
51. J. G. Herman, J. R. Graff, S. Myohanen, B. D. Nelkin, S. B. Baylin, Methylation-specific PCR: A novel PCR assay for methylation status of CpG islands. *Proc. Natl. Acad. Sci. U.S.A.* **93**, 9821–9826 (1996).
52. T. K. Wojdacz, The limitations of locus specific methylation qualification and quantification in clinical material. *Front. Genet.* **3**, 21 (2012).
53. H. H. Lai, C. Y. Yuan, H. Lin, Camber deformation property and fracture strain of flexible film made by polydimethylsiloxane. *Opt. Mater.* **107**, 110066 (2020).
54. B. F. Miller, T. R. Pisanic Ii, G. Margolin, H. M. Petrykowska, P. Athamanolap, A. Goncearenco, A. Osei-Tutu, C. M. Annunziata, T. H. Wang, L. Elnitski, Leveraging locus-specific epigenetic heterogeneity to improve the performance of blood-based DNA methylation biomarkers. *Clin Epigenetics* **12**, 154 (2020).
55. A. E. Teschendorff, J. West, S. Beck, Age-associated epigenetic drift: Implications, and a case of epigenetic thrift? *Hum. Mol. Genet.* **22**, R7–R15 (2013).
56. Y. Zhao, C. M. O'Keefe, K. Hsieh, L. Cope, S. C. Joyce, T. R. Pisanic, J. G. Herman, T.-H. Wang, Multiplex digital methylation-specific PCR for noninvasive screening of lung cancer. *Adv. Sci.* **10**, e2206518 (2023).
57. M. Li, W. D. Chen, N. Papadopoulos, S. N. Goodman, N. C. Bjerregaard, S. Laurberg, B. Levin, H. Juhl, N. Arber, H. Moinova, K. Durkee, K. Schmidt, Y. He, F. Diehl, V. E. Velculescu, S. Zhou, L. A. Diaz Jr., K. W. Kinzler, S. D. Markowitz, B. Vogelstein, Sensitive digital quantification of DNA methylation in clinical samples. *Nat. Biotechnol.* **27**, 858–863 (2009).
58. J. R. Molina, P. Yang, S. D. Cassivi, S. E. Schild, A. A. Adjei, Non-small cell lung cancer: Epidemiology, risk factors, treatment, and survivorship. *Mayo Clin. Proc.* **83**, 584–594 (2008).
59. The Lancet Respiratory Medicine, Lung cancer screening in Europe: Hurdles to overcome. *Lancet Respir. Med.* **6**, 885 (2018).
60. K. Ten Haaf, C. M. van der Aalst, H. J. de Koning, Clinically detected non-aggressive lung cancers: Implications for overdiagnosis and overtreatment in lung cancer screening. *Thorax* **73**, 407–408 (2018).
61. National Lung Screening Trial Research Team, D. R. Aberle, A. M. Adams, C. D. Berg, W. C. Black, J. D. Clapp, R. M. Fagerstrom, I. F. Gareen, C. Gatsonis, P. M. Marcus, J. R. D. Sicks, Reduced lung-cancer mortality with low-dose computed tomographic screening. *N. Engl. J. Med.* **365**, 395–409 (2011).
62. P. F. Pinsky, D. S. Gierada, P. H. Nath, E. Kazerooni, J. Amorosa, National lung screening trial: Variability in nodule detection rates in chest CT studies. *Radiology* **268**, 865–873 (2013).
63. L. S. Kinsinger, C. Anderson, J. Kim, M. Larson, S. H. Chan, H. A. King, K. L. Rice, C. G. Slatore, N. T. Tanner, K. Pittman, R. J. Monte, R. B. McNeil, J. M. Grubber, M. J. Kelley, D. Provenzale, S. K. Datta, N. S. Sperber, L. K. Barnes, D. H. Abbott, K. J. Sims, R. L. Whitley, R. R. Wu, G. L. Jackson, Implementation of lung cancer screening in the Veterans Health Administration. *JAMA Intern. Med.* **177**, 399–406 (2017).
64. D. E. Jonas, D. S. Reuland, S. M. Reddy, M. Nagle, S. D. Clark, R. P. Weber, C. Enyioha, T. L. Malo, A. T. Brenner, C. Armstrong, M. Coker-Schwimmer, J. C. Middleton, C. Voisin, R. P. Harris, Screening for lung cancer with low-dose computed tomography: Updated evidence report and systematic review for the US Preventive Services Task Force. *JAMA* **325**, 971–987 (2021).
65. L. Kreitmann, L. Miglietta, K. Xu, K. Malpartida-Cardenas, G. D'Souza, M. Kaforou, K. Brengel-Pesce, L. Drazek, A. Holmes, J. Rodriguez-Manzano, Next-generation molecular diagnostics: Leveraging digital technologies to enhance multiplexing in real-time PCR. *Trends Analyt. Chem.* **160**, 116963 (2023).
66. M. A. Keller, D. L. Cassel, E. F. Rappaport, S. E. McKenzie, E. Schwartz, S. Surrey, Fluorescence-based RT PCR analysis: Determination of the ratio of soluble to membrane-bound forms of Fc gamma RIIA transcripts in hematopoietic cell lines. *PCR Methods Appl.* **3**, 32–38 (1993).
67. P. M. Vallone, J. M. Butler, AutoDimer: A screening tool for primer-dimer and hairpin structures. *Biotechniques* **37**, 226–231 (2004).
68. K. A. Heyries, C. Tropini, M. Vaninsberghe, C. Doolin, O. I. Petriv, A. Singhal, K. Leung, C. B. Hughesman, C. L. Hansen, Megapixel digital PCR. *Nat. Methods* **8**, 649–651 (2011).
69. J. Lu, A. Johnston, P. Berichon, K. L. Ru, D. Korbie, M. Trau, PrimerSuite: A high-throughput web-based primer design program for multiplex bisulfite PCR. *Sci. Rep.* **7**, 41328 (2017).
70. G. E. Tusnady, I. Simon, A. Varadi, T. Aranyi, BiSearch: Primer-design and search tool for PCR on bisulfite-treated genomes. *Nucleic Acids Res.* **33**, e9 (2005).
71. D. S. Ettinger, D. E. Wood, W. Akerley, L. A. Bazhenova, H. Borghaei, D. R. Camidge, R. T. Cheney, L. R. Chirieac, T. A. D'Amico, T. L. Demmy, T. J. Dilling, R. Govindan, F. W. Grannis Jr., L. Horn, T. M. Jahan, R. Komaki, M. G. Kris, L. M. Krug, R. P. Lackner, M. Lanuti, R. Lilenbaum, J. Lin, B. W. Loo Jr., R. Martins, G. A. Otterson, J. D. Patel, K. M. Pisters, K. Reckamp, G. J. Riely, E. Rohren, S. Schild, T. A. Shapiro, S. J. Swanson, K. Tauer, S. C. Yang, K. Gregory, M. Hughes, Non-small cell lung cancer, version 1.2015. *J. Natl. Compr. Canc. Netw.* **12**, 1738–1761 (2014).

Acknowledgments: We appreciate Y. Guo for contributing to data analysis. **Funding:** This work was supported by the National Institutes of Health/National Cancer Institute (R01CA260628, R33CA272321, and P50CA22899), the Break Through Cancer Foundation, and the NIH Early Detection Research Network (U01CA214165, U2CCA271885, and CFAM2019-08).
Author contributions: Conceptualization: T.-H.W., T.R.P., and J.G.H. Methodology: Y.Z., T.-H.W., and T.R.P. Software: C.M.O. and Y.Z. Validation: W.C., C.M.A., and H.L. Formal analysis: Y.Z. and C.M.O. Investigation: Y.Z., J.H., W.C., A.C., C.M.A., and H.L. Resources: S.C.J. and J.G.H. Data curation: Y.Z. and C.M.O. Visualization: Y.Z. Supervision: T.-H.W., T.R.P., and J.G.H. Project administration: T.-H.W. Writing—original draft: Y.Z. and T.R.P. Writing—review and editing: Y.Z., T.R.P., T.-H.W., K.H., and J.G.H. **Competing interests:** The authors declare that a patent application related to the content of this manuscript has been submitted. The authors declare that they have no other competing interests. **Data and materials availability:** All data needed to evaluate the conclusions in the paper are present in the paper and/or the Supplementary Materials.

Submitted 12 March 2024
Accepted 22 October 2024
Published 22 November 2024
10.1126/sciadv.adp1704